Controlling thermal conductance through quantum dot roughening at interfaces

Patrick E. Hopkins,[1,2,*] John C. Duda,[1,2] Christopher W. Petz,[3] and Jerrold A. Floro[3]
[1]*Department of Mechanical and Aerospace Engineering, University of Virginia, Charlottesville, Virginia, USA 22904*
[2]*Engineering Sciences Center, Sandia National Laboratories, Albuquerque, New Mexico, USA 87185*
[3]*Department of Materials Science and Engineering, University of Virginia, Charlottesville, Virginia, USA 22904*
(Received 19 January 2011; revised manuscript received 5 April 2011; published 27 July 2011)

We examine the fundamental phonon mechanisms affecting the interfacial thermal conductance across a single layer of quantum dots (QDs) on a planar substrate. We synthesize a series of Ge_xSi_{1-x} QDs by heteroepitaxial self-assembly on Si surfaces and modify the growth conditions to provide QD layers with different root-mean-square (rms) roughness levels in order to quantify the effects of roughness on thermal transport. We measure the thermal boundary conductance (h_K) with time-domain thermoreflectance. The trends in thermal boundary conductance show that the effect of the QDs on h_K are more apparent at elevated temperatures, while at low temperatures, the QD patterning does not drastically affect h_K. The functional dependence of h_K with rms surface roughness reveals a trend that suggests that both vibrational mismatch and changes in the localized phonon transport near the interface contribute to the reduction in h_K. We find that QD structures with rms roughnesses greater than 4 nm decrease h_K at Si interfaces by a factor of 1.6. We develop an analytical model for phonon transport at rough interfaces based on a diffusive scattering assumption and phonon attenuation that describes the measured trends in h_K. This indicates that the observed reduction in thermal conductivity in SiGe quantum dot superlattices is primarily due to the increased physical roughness at the interfaces, which creates additional phonon resistive processes beyond the interfacial vibrational mismatch.

DOI: 10.1103/PhysRevB.84.035438 PACS number(s): 66.70.−f, 66.90.+r, 68.65.Hb

I. INTRODUCTION

Successful reductions in the thermal conductivities of nanosystems have been achieved through the alteration of structure and interface density in different types of nanoparticle films and periodic composites.[1–13] These material systems have attracted significant attention due to their unique phonon-scattering mechanisms, where the increase in the density of inclusions increases the number and frequency of boundary scattering events, in turn resulting in lower realized values of effective thermal conductivity. Thus, through varying the frequency and strength of phonon scattering at interfaces, one is able to obtain a unique method for controlling the effective thermal conductivity of a given nanosystem. This concept is of great interest for applications involving thermoelectric cooling and power generation,[14–16] and thermal insulation.[17] In addition, this concept has far-reaching implications in the area of solid-state thermal rectification[18–21] and asymmetric heat conduction[22,23] for advanced technologies such as thermal transistors[24] or thermal storage devices.[25]

Recent works have examined the effects of SiGe-based quantum dot (QD) superlattices in an attempt to further reduce the thermal conductivities of SiGe material systems.[11,26,27] These efforts have collectively determined that QD patterning at interfaces drastically reduces the overall thermal conductivity of SiGe superlattice materials. The recent work by Pernot *et al.*[11] further demonstrated the "tunability" of this reduction in thermal conductivity by precise control over superlattice period and QD areal density. They attributed this control to diffusive scattering at the QD covered interfaces. However, the notion of diffusive interface scattering largely encompasses a broad domain of phonon transport processes. Therefore, the fundamental phononic mechanisms driving the reduction in the cross-plane thermal conductivity of quantum dot superlattices remain controversial[27] and include acoustic impedance mismatch scattering, phonon localization and attenuation, and alteration of phonon dispersion relations.[28]

In this paper, we examine fundamental phonon mechanisms affecting the thermal conductance of QD superlattices by studying the thermal boundary conductance, or Kapitza conductance (h_K), across a single layer of QDs on a planar substrate. We synthesize a series of Ge_xSi_{1-x} QDs by heteroepitaxial self-assembly on Si surfaces and metallize (aluminum) the surface to study how the QDs affect the heat transport across interfaces. Growth conditions are modified to provide QD layers with different root-mean-square (rms) roughness levels in order to quantify the effects of roughness on thermal transport. We measure the thermal boundary conductance with time-domain thermoreflectance (TDTR).[29,30] The trends in thermal boundary conductance show that the effect of the QDs on h_K are more apparent at elevated temperatures, while at low temperatures, the QD patterning does not drastically affect h_K. The functional dependence of h_K with rms surface roughness reveals a trend that suggests that both the vibrational mismatch and an additional localized phonon processes near the interface contribute to the reduction in h_K. We develop an analytical model for phonon thermal transport across rough interfaces based on a diffusive scattering assumption and phonon attenuation that describes the measured trends in h_K. This indicates that the observed reduction in thermal conductivity in SiGe QD superlattices is primarily due to the increased physical roughness at the interfaces, which creates additional phonon resistive mechanisms beyond the interfacial vibrational mismatch.

II. EXPERIMENTAL DETAILS

The growth of the various QD roughened Si surfaces begins with heteroepitaxial growth of Ge_xSi_{1-x} via the Stranski-Krastanow growth mode.[31] The alloy layer

 ©2011 American Physical Society

TABLE I. Growth and characterization information of the QD samples.

Fig.	Ge atom fraction	Thickness (nm)	Growth temperature (°C)	Growth rate (nm s^{-1})	Density (QDs μm^{-2})	rms roughness (nm)
1(a)	1.0	0.70	550	0.010	96	0.28
1(b)	1.0	0.85	550	0.010	590	0.53
1(c)	1.0	0.85	600	0.010	75	1.38
1(d)	0.5	2.60	740	0.017	55	2.16
1(e)	0.5	3.10	740	0.017	36	4.46

initially grows planar on the Si(001) surface, but above some wetting-layer thickness, subsequent material forms coherent three-dimensional (3D) islands to partially relieve the lattice mismatch strain (given by $\epsilon_{mis} = 0.04x$). Initially, "pyramid" islands form exhibiting fourfold-symmetric {105} facets, and with continued GeSi deposition, larger dome-shaped islands evolve with dominant {113} facets.[32–34] Pyramid and dome size and areal density may be modified (thereby varying the surface roughness) by controlling the composition, film thickness, and growth kinetics, e.g., substrate temperature (T_s) and deposition rate (R_g).[33,35,36]

$Ge_xSi_{1-x}/Si(001)$ QDs are grown via ultrahigh vacuum molecular beam epitaxy (MBE) (base pressure = 10^{-10} Torr). Prior to insertion to the MBE, Si wafers are chemically cleaned via a standard IMEC/Shiraki process to remove hydrocarbon and transition-metal impurities, creating in the final step a passive SiO_x layer. Si(001) substrates, with a miscut of $+/-0.1°$, are outgassed in the MBE at 600 °C for greater than 10 h, ramped to 850 °C over 30 min to desorb the oxide layer, and cooled to 700 °C for deposition of a 50-nm Si buffer layer. Throughout this process, the surface structure is monitored with reflection high-energy electron diffraction (RHEED) to ensure 2×1 surface reconstruction. We deposit Ge and Si with magnetron sputtering in 3 mTorr of getter-purified Ar. Once a clean surface is obtained, Ge(GeSi) heteroepitaxy proceeds. After growth, surface morphology is characterized *ex situ* by atomic-force microscopy (AFM) (NT-MDT Solver Pro M) using NSG10 tips with radius less than 10 nm. The growth parameters, observed surface features, and representative line features for each film are summarized in Table I and Fig. 1. The representative line scans are taken around the vicinity QDs to make clear the difference in surface features among the different samples. The rms roughness values (δ) are calculated from 4-, 2-, and 1-μm^2 micrographs and represent less than 4% error. Prior to metallization, we clean the substrate with methanol and acetone and dry with nitrogen. We then evaporate 90 nm of Al on the QD roughened Si surfaces at a vacuum pressure of 3.7×10^{-7} Torr.

We measured the thermal boundary conductance across the QD structurally variant Al/Si interfaces with TDTR.[29,30] TDTR is a noncontact, pump-probe technique in which a modulated train of short laser pulses (in our case, ~100 fs)

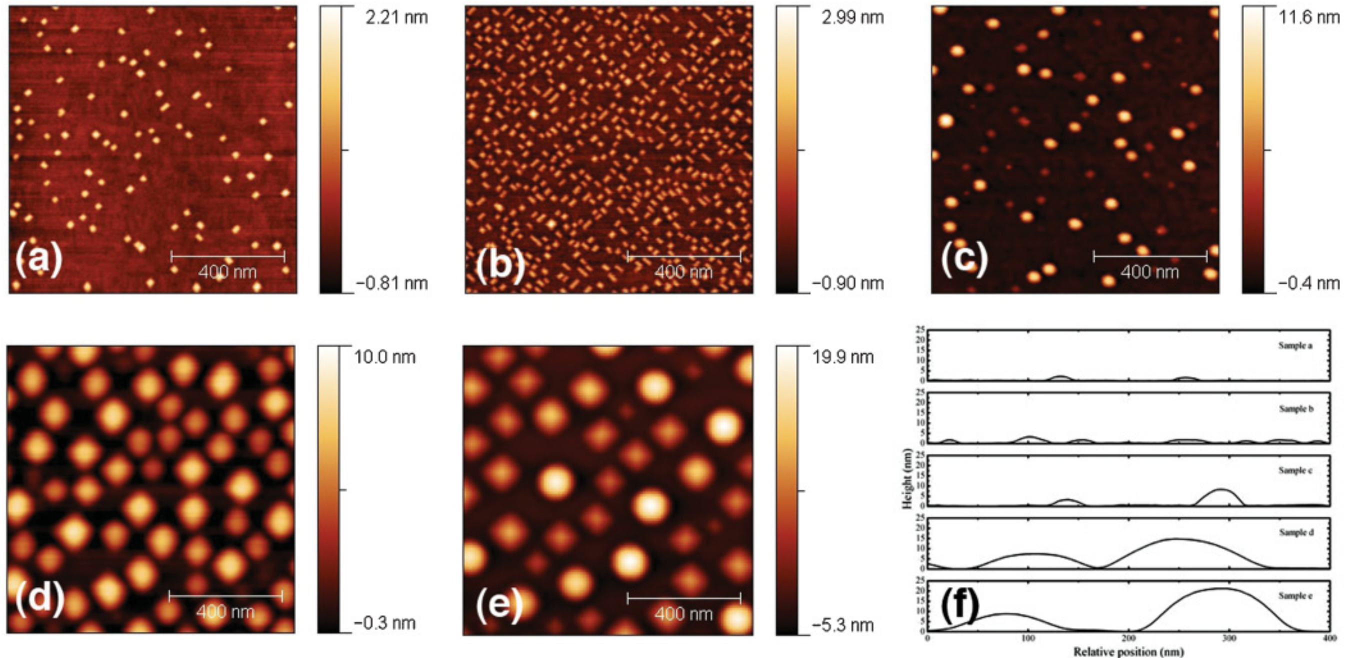

FIG. 1. (Color online) Atomic-force microscrope images and representative line scans of the QD roughened surfaces studied in this paper. These specific surfaces have rms roughnesses of (a) 0.28 nm from Ge QDs, (b) 0.53 nm from Ge QDs, (c) 1.38 nm from Ge QDs, (d) 2.16 nm from GeSi QDs, and (e) 4.46 nm from GeSi QDs. The representative line scans of each AFM are shown in (f). Further growth information is given in Table I.

is used to create a heating event (pump) on the surface of a sample. This pump-heating event is then monitored with a time-delayed probe pulse. The change in the reflectivity of the probe pulses at the modulation frequency of the pump train is detected through a lock-in amplifier; this change in reflectivity is related to the temperature change on the surface of the sample. These temporal temperature data are related to the thermophysical properties of the sample of interest. We monitor the thermoreflectance signal over 4.5 ns of probe delay time. The deposited energy takes approximately 100 ps to propagate through the Al layer, and the remaining delay time is related to the heat flow across the Al/Si interface. Our specific experimental setup is described in detail elsewhere.[37]

The thermoreflectance signal we monitor is the ratio of the in-phase to the out-of-phase voltage recorded by the lock-in amplifier ($-V_{\rm in}/V_{\rm out}$), which is related to the temperature change on the surface of the sample. The thermal model and analysis used to predict the temperature change and subsequent lock-in ratio is described in detail in the references.[29,37,38] In short, the thermal model accounts for heat transfer in composite slabs[39] from a periodic, Gaussian source (pump) convoluted with a Gaussian sampling spot (probe).[29,40] In our experiments, our pump modulation frequency is 11 MHz and our pump and probe $1/e^2$ radii are 7.5 μm. The temperature change at the surface is related to the thermal conductivity κ and heat capacity C of the composite slabs and $h_{\rm K}$ between each slab. Although dominated by the Al/Si thermal interface conductance,[37] the TDTR signal is also related to the heat capacity and thickness of the Al film and the thermal properties of the Si substrate (which, due to time delay and modulation frequency considerations, can be assumed as semi-infinite in this paper). We assume bulk values for the thermophysical properties of the Al and Si,[41] and we verify the Al film thickness via picosecond ultrasonics.[42,43] We adjust the thermal conductivity of the substrate during our analysis to achieve a better fit between the model and the data.[44]

III. RESULTS

Figure 2 shows the measured thermal conductance across the various Al/Si interfaces as a function of temperature. The control sample (no QD patterning, $\delta = 0.08$ nm) has the highest conductance. The general trend among the data indicate that the conductance decreases due to the physical surface roughness associated with the QD topography, even at surface roughnesses less than 1 nm. Also, note that the values for conductance converge at low temperatures. This is due to the fact that the magnitude of the surface roughness selectively scatters only certain phonons with wavelengths less than the characteristic roughness produced by the QDs, a potential avenue for control of thermal interface conductance based on the magnitude of the roughness. The phonon-scattering mechanisms at these rough QD interfaces are quantified and discussed in the remainder of this paper.

To better understand phonon transport across roughened interfaces, we turn to interfacial modeling via the diffuse mismatch model (DMM).[45] The DMM makes the assumption that all phonons approaching an interface between two materials must scatter diffusively. The drastic change in lattice periodicity from one material to another will cause scattering at the interface, thereby restricting phonon mean-free paths to the interfacial scattering events. The diffusive nature of this interfacial scattering event is justified at elevated temperatures ($T > 50$ K) due to phonon wavelength considerations.[46] For DMM calculations, we use the exact phonon dispersion in a given crystallographic direction and employ an isotropic assumption when describing the phononic properties of Al and Si.[46] That is, we assume isotropic dispersion based on that in the [100] direction for both Al and Si from Refs. 47 and 48, respectively. We have previously shown that this isotropic dispersion assumption is acceptable for predicting interface conductance across junctions between cubic crystals and yields a much improved prediction over traditional Debye approaches.[46]

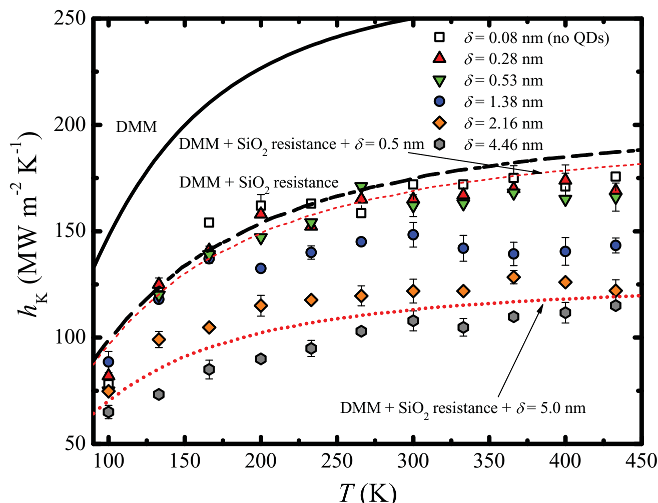

FIG. 2. (Color online) Measured thermal conductance of the six Al/Si interfaces fabricated in this work as a function of temperature. The QD patterning on the surface of the Si causes reduction in $h_{\rm K}$. In addition, the measured $h_{\rm K}$ on the six samples converges at low temperature, indicating that phonons are not as readily affected by the roughness at low temperatures, indicative of longer-wavelength phonon-dominated transport. Also shown in this figure are calculations of the DMM. Accounting for the thermal resistance associated with the native oxide layer on the surface of the Si greatly improves the agreement between the DMM and the Al/Si interface with no QD patterning. The roughness is accounted for by assuming that short-wavelength phonons are more readily scattered at rough interfaces that have greater coverage of QDs, as described by Eq. (8). We plot the DMM using the phonon attenuation parameter given in Eq. (8) as the dashed lines assuming a QD rms roughness of $\delta = 0.5$ or 5.0 nm. Our model that accounts for additional phonon attenuation by the QDs agrees well in both value and trend as the corresponding data with similar rms roughnesses.

Under the isotropic assumption, the phonon flux transmitted across the interface from the Al to the Si and is given as

$$q_{1\to 2} = \frac{1}{8\pi^2}\sum_j \int_{k_{1,\max}} (\hbar\omega_j(k_1)\,k_1^2 \times \zeta^{1\to 2}\,|v_{1,j}(k_1)|\,f\,dk_1), \quad (1)$$

where k is the wave vector, $k_{\max}$ is the maximum wave vector, ω is the phonon angular frequency, $\zeta^{1\to 2}$ is the transmission

probability from side 1 (Al) to side 2 (Si), v_1 is phonon group velocity in the Al and equal to $\partial\omega/\partial k$, f is the phonon distribution function, which in this paper we assume as the equilibrium Bose-Einstein distribution, and j is polarization (e.g., longitudinal acoustic or transverse acoustic). Recognizing that $q_{1\to 2} = h_{\mathrm{K}}\Delta T$, the thermal boundary conductance is given by[49]

$$h_{\mathrm{K},1\to 2} = \frac{1}{8\pi^2}\sum_j \int_{k_{1,\max}} \left(\hbar\omega_j(k_1)\,k_1^2 \times \zeta^{1\to 2}\,|v_{1,j}(k_1)|\,\frac{\partial f}{\partial T}\,dk_1\right). \quad (2)$$

We assume that the phonons are scattered elastically at the interface[46] so that frequencies only up to the maximum frequency in Al are considered. To calculate the transmission coefficient, we apply detailed balance on the fluxes crossing the interface from the Al and from the Si and apply the definition of diffuse scattering (i.e., $\zeta^{1\to 2} = 1 - \zeta^{2\to 1}$) to yield[46]

$$\zeta_{1\to 2} = \frac{\sum_j k_2^2}{\sum_j k_1^2 + \sum_j k_2^2}, \quad (3)$$

where the transmission at each phonon frequency, regardless of polarization, is calculated consistent with our assumptions during evocation of detailed balance and calculation of Eq. (2), namely, elastic scattering.[50] Therefore, under the isotropic and diffuse assumptions, h_{K} as calculated via the DMM is given as

$$h_{\mathrm{K,DMM}} = \frac{1}{8\pi^2}\sum_j \int_{k_{1,\max}} \left(\hbar\omega_j(k_1)\,k_1^2 \times \frac{\sum_j k_2^2}{\sum_j k_1^2 + \sum_j k_2^2}\,|v_{1,j}(k_1)|\,\frac{\partial f}{\partial T}\,dk_1\right). \quad (4)$$

The calculations of the DMM as a function of temperature are labeled as "DMM" in Fig. 2. These predictions clearly overestimate the measured data on our smoothest sample with no QD patterning. Another resistance that must be accounted for at these interfaces is the resistance associated with the native oxide layer on the sample surface. In our previous paper,[51] we determined that the thermal resistance associated with the native oxide can be approximated as the thickness of the native oxide layer divided by the thermal conductivity of corresponding amorphous bulk phase. The conductance of this layer is then

$$h_{\mathrm{oxide}} = \frac{\kappa_{\mathrm{oxide}}}{t_{\mathrm{oxide}}}, \quad (5)$$

where t is the native-oxide-layer thickness which we approximate as 2.5 nm from transmission electron microscopy analysis on Al/Si interfaces, and we assume the thermal conductivity of the native oxide layer is given by that of bulk SiO_2,[52] so that the effective conductance of the Al/Si interface with a native oxide layer on the sample surface is given by

$$h_{\mathrm{K}} = \left(h_{\mathrm{K,DMM}}^{-1} + h_{\mathrm{oxide}}^{-1}\right)^{-1}. \quad (6)$$

Note that, for these calculations, we use the thermal conductivity of SiO_2. Although there may also be some formation of germania in the native oxide layer, the thermal conductivity of vitreous Si and Ge are similar at elevated temperatures,[53] so germania in the native oxide layer should not significantly affect our calculations. The DMM predictions when accounting for a native oxide layer are in much better agreement with our Al/Si interface than the corresponding predictions without the native-oxide-layer resistance. The increase at higher temperatures in the model is due to our assumption that the SiO_2 conductance follows the temperature dependency of thicker, amorphous SiO_2. However, the agreement between our DMM calculations and our measured Al/Si interface conductance suggests that the DMM is a suitable model to explore the phonon processes participating in thermal conductance at Al/Si interfaces in the temperature range of interest in this paper. Furthermore, this suggests that phonons are scattering diffusely at the temperatures of interest in this study and the interface conductance is driven by the vibrational mismatch between the Al and Si, which manifests itself as a mismatch of phonon density of states. However, the DMM with the additional native oxide resistance does not explain the variation in h_{K} that we observe with QD patterning and roughness.

IV. MODELING THERMAL TRANSPORT ACROSS ROUGH INTERFACES

In this paper, our Ge_xSi_{1-x}/Si materials and interfaces are fully crystalline and coherent, but covered by a native oxide. The Al layer is polycrystalline, but intermixing is suppressed by the low growth temperature and the presence of the SiO_2. Thus, we take the view that the self-assembled quantum dots affect thermal boundary conductance only via mechanisms induced by the topographic roughness, but do not otherwise have a unique vibrational identity. We discuss the veracity of this assumption later. Previous works have modeled phonon transport across heterointerfaces incorporating nonidealities such as extended chemical intermixing,[51,54,55] misfit dislocations,[56,57] and microcrystalline or amorphous regions.[58–60] In all of these previous works, changes in h_{K} were controlled by changes in the diffusive phonon-scattering events around the interface caused by these nonidealities.

To account for the various scattering events at the QD-patterned interfaces, we introduce an "attenuation-type" model, similar to the Beer-Lambert law of photon attenuation. In this case, we introduce a "roughness factor" γ in the thermal boundary conductance in Eq. (4), so that the DMM is calculated by

$$h_{\mathrm{K,DMM}} = \frac{1}{8\pi^2}\sum_j \int_{k_{1,\max}} \left(\gamma\,\hbar\omega_j(k_1)\,k_1^2 \times \frac{\sum_j k_2^2}{\sum_j k_1^2 + \sum_j k_2^2}\,|v_{1,j}(k_1)|\,\frac{\partial f}{\partial T}\,dk_1\right). \quad (7)$$

In Eq. (7), γ accounts for the geometric roughness of the interface and is related to the phonon attenuation events

due to the finite roughness. We define this roughness factor as

$$\gamma = \begin{cases} 1, & \lambda > \delta \\ \exp\left[-\left(\frac{4\pi\beta}{\lambda}\right)\delta\right], & \lambda < \delta \end{cases} \quad (8)$$

where λ is the phonon wavelength and we define β as the unitless phonon "attenuation constant" of the interface (for a perfect interface, $\beta \rightarrow 0$), and δ is the rms roughness of the interface. Note that the phonon wavelength λ is related to the phonon wave vector k, and therefore this expression is inserted into the integrand of Eq. (7). In Eq. (8), the term $4\pi\beta/\lambda$ exactly parallels the linear attenuation coefficient of photons as described by the Beer-Lambert law. The piecewise definition of the model describes a scenario in which phonons with wavelengths longer than δ do not "see" the rough region, and therefore their interfacial conductance is governed by that predicted by the DMM. On the other hand, the degree to which phonons with wavelengths shorter than δ are attenuated by this region depends on the relative values of λ and δ, and the phonons propagating in this region are attenuated by γ. This wavelength dependency of thermal boundary conductance has been previously observed at grain boundaries with only a few monolayers of roughness using molecular dynamics simulations.[61]

To examine the effect of interface roughness on h_K, we plot h_K as a function of δ at 300 K for the six samples measured in this study in Fig. 3. Calculations of Eq. (7) at $T = 300$ K as a function of δ are also shown in Fig. 3. Note that in these calculations we also account for the native oxide layer via Eq. (6). We use β as a fitting parameter to account for the various scattering mechanisms at the QD patterned interfaces that can be leading to phonon attenuation. We find that a single value of $\beta = 0.0040$ leads to a good agreement between the model and experimental data, especially for small values of rms roughness, indicating that phonons are being attenuated by similar mechanisms at the various Al/QD/Si interfaces. The model given in Eqs. (7) and (8) assumes that phonons are diffusely scattered at the Al/Si interface via processes described by the DMM. It also accounts for the interfacial flux that is additionally attenuated by the scattering of short-wavelength phonons via the structure around the interface. This short-wavelength phonon attenuation drives the trend in h_K with interfacial roughness. Note that the material comprising the interface structure, i.e., Ge or GeSi, does not enter into the formulation of this model. This indicates that the heat flow is strongly dictated by the differences in the phonon density of states between the Al and the Si, while topographical roughness at the interface causes additional phonon attenuation. The excellent fit to the data indicates that the limited amount of Ge on the Si surface does not have a vibrational identity distinguishable from that of the substrate.

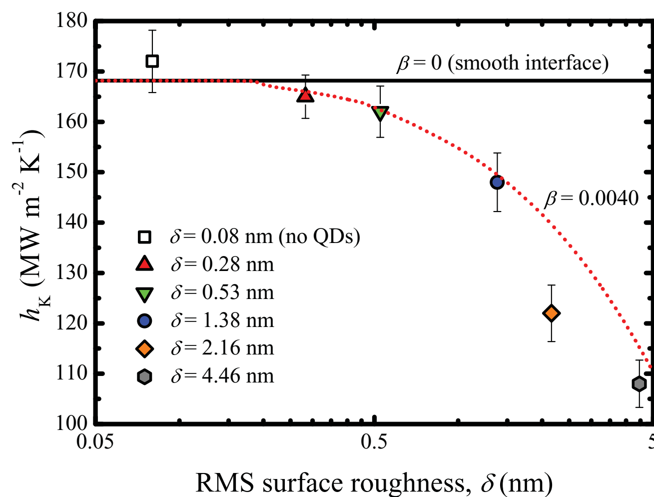

FIG. 3. (Color online) Thermal conductance as a function of rms roughness across the series of structurally variant Al/Si interfaces at 300 K. Calculations of Eq. (7) at $T = 300$ K as a function of δ are also shown. We find that $\beta = 0.0040$ leads to a good agreement between the model and experimental data.

We also show predictions of Eq. (7) for a rms roughness of 0.5 and 5 nm in Fig. 2 assuming $\beta = 0.0040$; these predictions capture the temperature-dependent reduction in h_K due to roughness relatively well with a single value of β. In addition, note that the roughness models begin to converge at low temperatures, a similar trend as is observed in the experimental data. This is due to the fact that, at low temperatures, the thermal flux has a higher population of phonons with wavelengths greater than δ as compared to elevated (room) temperatures; consequently, these long-wavelength phonons do not "see" the interfacial features and are scattered from DMM-type considerations alone (i.e., mismatch in phonon density of states). We note that this sound agreement between our data and this attenuation-based phonon transport model is achieved with only one fitting parameter. This idea of interfacial phonon attenuation is captured with our relatively simple, analytical model and agrees well with our quantum dot roughened interfaces, despite the fact that these interfaces exhibit a wide range of lateral length scales and represent nanostructured roughness rather than random atomic roughness.

To further validate this model, we use this description of phonon attenuation to predict the effective thermal conductivity of a QD superlattice as measured by Pernot *et al.*[11] The Ge QD-patterned Si/Si interfaces in that study were characterized as having a 70% QD coverage area with an average feature height of 1.2 nm, corresponding to a rms roughness of approximately 1 nm. According to our above description of phonon transport at QD patterned interfaces, the Ge QD arrays at each interface do not have significant vibrational identities of their own. Therefore, we calculate our predictions of interface conductance for a single Ge QD patterned Si/Si interface using the same bulk phonon dispersion of Si described above.[48] We use $\beta = 0.0040$ to stay consistent with our above calculations. At room temperature, the model predicts an individual interface conductance of 255 MW m^{-2} K^{-1} at 300 K, which is in excellent agreement with the value inferred by Pernot *et al.* (between 250 and 500 MW m^{-2} K^{-1}). Assuming the bulk thermal conductivity of Si at 300 K, $\kappa_{Si} = 148$ W m^{-1} K^{-1}, and using the described interface spacing L, where $L = 12.8$ nm, an effective thermal conductivity can be calculated through

consideration of the individual conductances (interface and bulk) and the effective length scale L given by

$$\kappa_{\mathrm{eff}} = L\left[h_{\mathrm{K}}^{-1} + \left(\frac{\kappa_{\mathrm{Si}}}{L}\right)^{-1}\right]^{-1}. \quad (9)$$

Equation (9) yields $\kappa_{\mathrm{eff}} = 3.2$ W m^{-1} K^{-1} at 300 K, which is again in excellent agreement with the two reported measurements of Pernot *et al.*, i.e., 3.7 ± 0.85 W m^{-1} K^{-1} and 3.4 ± 0.50 W m^{-1} K^{-1}.

The fact that a single attenuation constant accurately describes phonon transport across the various silicon interfaces in this work and that of Pernot *et al.*[11] lends insight into the phonon-scattering processes driving thermal boundary conductance at roughened interfaces. The attenuation coefficient for phonons introduced in this paper, given by $4\pi\beta/\lambda$, exactly parallels its photonic counterpart, thereby representing the total loss of the phonon flux at the interface. For phonons, this represents additional losses in phonon intensity that decrease the heat flow across the interface. Given the rough features from QD synthesis on a Si surface, the incident phonon flux is affected by the mismatch between the phonon flux and the phonon density of states in the Si and further attenuated by the presence of vibrationally unidentifiable features at the interface. As the phonon attenuation exists only at a few nanometers around the interface, this implies that the roughened features localized the phonon attenuation near the interface, indicating that both phonon localization effects and vibrational mismatch between two materials are the fundamental phononic mechanisms driving the reduction in the cross-plane thermal conductivity of quantum dot superlattices.

V. SUMMARY

In summary, we find that QD roughening at Si interfaces decreases the thermal conductance via localized phonon attenuation beyond vibrational mismatch resistance. The trends in thermal boundary conductance between Al and Si show that the effect of the QDs on phonon scattering are more apparent at elevated temperatures, while at low temperatures, the QD patterning does not drastically affect h_{K}. We find that QD structures with rms roughnesses greater than 4 nm decrease h_{K} at Si interfaces by a factor of 1.6. We develop an analytical model for phonon attenuation at rough interfaces, showing that the observed reduction in the cross-plane thermal conductivity of QD superlattices is due to diffusive scattering driven by vibrational mismatch and phonon localization at the superlattice interfaces.

ACKNOWLEDGMENTS

P.E.H. is appreciative for funding from the LDRD program office through the Sandia National Laboratories Harry S. Truman Fellowship Program. J.C.D. is appreciative for funding from the National Science Foundation Graduate Research Fellowship Program. We would also like to thank Joseph Kassim for additional MBE growth. This work was performed, in part, at the Center for Integrated Nanotechnologies, a US Department of Energy, Office of Basic Energy Sciences user facility. Sandia is a multiprogram laboratory operated by Sandia Corporation, a wholly owned subsidiary of Lockheed Martin Corporation, for the United States Department of Energy's National Nuclear Security Administration under Contract No. DE-AC04-94AL85000.

[*]Corresponding author: phopkins@virginia.edu

[1]W. Kim, J. Zide, A. Gossard, D. Klenov, S. Stemmer, A. Shakouri, and A. Majumdar, Phys. Rev. Lett. **96**, 045901 (2006).

[2]G. Zeng, J. H. Bahk, J. E. Bowers, J. M. O. Zide, A. C. Gossard, Z. Bian, R. Singh, A. Shakouri, W. Kim, S. L. Singer, and A. Majumdar, Appl. Phys. Lett. **91**, 263510 (2007).

[3]Y. K. Koh, S. L. Singer, W. Kim, J. M. O. Zide, H. Lu, D. G. Cahill, A. Majumdar, and A. C. Gossard, J. Appl. Phys. **105**, 054303 (2009).

[4]X. J. Hu, R. Prasher, and K. Lofgreen, Appl. Phys. Lett. **91**, 203113 (2007).

[5]R. M. Costescu, D. G. Cahill, F. H. Fabreguette, Z. A. Sechrist, and S. M. George, Science **303**, 989 (2004).

[6]C. Chiritescu, D. G. Cahill, N. Nguyen, D. Johnson, A. Bodapati, P. Keblinski, and P. Zschack, Science **315**, 351 (2007).

[7]J. H. Lee, G. A. Galli, and J. C. Grossman, Nano Lett. **8**, 3750 (2008).

[8]R. S. Prasher, Phys. Rev. B **74**, 165413 (2006).

[9]R. Venkatasubramanian, E. Siivola, T. Colpittas, and B. O'Quinn, Nature (London) **413**, 597 (2001).

[10]S. M. Lee, D. G. Cahill, and R. Venkatasubramanian, Appl. Phys. Lett. **70**, 2957 (1997).

[11]G. Pernot, M. Stoffel, I. Savic, F. Pezzoli, P. Chen, G. Savelli, A. Jacquot, J. Schumann, U. Denker, I. Monch, C. Deneke, O. G. Schmidt, J. M. Rampnoux, S. Wang, M. Plissonnier, A. Rastelli, S. Dilhaire, and N. Mingo, Nat. Mater. **9**, 491 (2010).

[12]J. K. Yu, S. Mitrovic, D. Tham, J. Varghese, and J. R. Heath, Nat. Nanotechnol. **5**, 718 (2010).

[13]S. T. Huxtable, A. R. Abramson, C. L. Tien, A. Majumdar, C. LaBounty, X. Fan, G. Zeng, J. E. Bowers, A. Shakouri, and E. T. Croke, Appl. Phys. Lett. **80**, 1737 (2002).

[14]B. Poudel, Q. Hao, Y. Ma, L. Yucheng, A. Minnich, B. Yu, X. Yan, D. Wang, A. Muto, D. Vashaee, X. Chen, J. Liu, M. S. Dresselhaus, G. Chen, and Z. Ren, Science **320**, 634 (2008).

[15]L. E. Bell, Science **321**, 1457 (2008).

[16]T. C. Harman, P. J. Taylor, M. P. Walsh, and B. E. LaForge, Science **297**, 2229 (2002).

[17]N. P. Padture, M. Gell, and E. H. Jordan, Science **296**, 280 (2002).

[18]P. E. Hopkins and J. R. Serrano, Phys. Rev. B **80**, 201408(R) (2009).

[19]W. Kobayashi, Y. Teraoka, and I. Terasaki, Appl. Phys. Lett. **95**, 171905 (2009).

[20]J. N. Miller, W. Jang, and C. Dames, in Proceedings of the ASME 2009 Heat Transfer Summer Conference (ASME, New York, 2009), p. 88488.

[21]C. W. Chang, D. Okawa, A. Majumdar, and A. Zettl, Science **314**, 1121 (2006).
[22]B. Hu, L. Yang, and Y. Zhang, Phys. Rev. Lett. **97**, 124302 (2006).
[23]D. Segal, Phys. Rev. E **79**, 012103 (2009).
[24]B. Li, L. Wang, and G. Casati, Appl. Phys. Lett. **88**, 143501 (2006).
[25]L. Wang and B. Li, Phys. Rev. Lett. **101**, 267203 (2008).
[26]B. Yang, J. L. Liu, K. L. Wang, and G. Chen, Appl. Phys. Lett. **80**, 1758 (2002).
[27]M. L. Lee and R. Venkatasubramanian, Appl. Phys. Lett. **92**, 053112 (2008).
[28]D. G. Cahill, W. K. Ford, K. E. Goodson, G. D. Mahan, A. Majumdar, H. J. Maris, R. Merlin, and S. R. Phillpot, J. Appl. Phys. **93**, 793 (2003).
[29]D. G. Cahill, Rev. Sci. Instrum. **75**, 5119 (2004).
[30]D. G. Cahill, K. E. Goodson, and A. Majumdar, J. Heat Transfer **124**, 223 (2002).
[31]D. J. Eaglesham and M. Cerullo, Phys. Rev. Lett. **64**, 1943 (1990).
[32]G. Medeiros-Ribeiro, A. M. Bratkovski, T. I. Kamins, D. A. Ohlberg, and R. S. Williams, Science **279**, 353 (1998).
[33]T. Kamins, G. Medeiros-Ribeiro, D. Ohlberg, and R. S. Williams, Appl. Phys. A: Mater. Sci. Process. **67**, 727 (1998).
[34]F. M. Ross, J. Tersoff, and R. M. Tromp, Phys. Rev. Lett. **80**, 984 (1998).
[35]B. Cho, T. Schwarz-Selinger, K. Ohmori, D. G. Cahill, and J. E. Greene, Phys. Rev. B **66**, 195407 (2002).
[36]M. W. Dashiell, U. Denker, C. Muller, G. Costantini, C. Manzano, K. Kern, and O. G. Schmidt, Appl. Phys. Lett. **80**, 1279 (2002).
[37]P. E. Hopkins, J. R. Serrano, L. M. Phinney, S. P. Kearney, T. W. Grasser, and C. T. Harris, J. Heat Transfer **132**, 081302 (2010).
[38]A. J. Schmidt, X. Chen, and G. Chen, Rev. Sci. Instrum. **79**, 114902 (2008).
[39]H. S. Carslaw and J. C. Jaeger, *Conduction of Heat in Solids,* 2nd ed. (Oxford University, New York, 2003), pp. 109–112.
[40]H. S. Carslaw and J. C. Jaeger, *Conduction of Heat in Solids,* 2nd ed. (Oxford University, New York, 2003), p. 263.
[41]C. Y. Ho, R. W. Powell, and P. E. Liley, J. Phys. Chem. Ref. Data **1**, 279 (1972).
[42]C. Thomsen, H. T. Grahn, H. J. Maris, and J. Tauc, Phys. Rev. B **34**, 4129 (1986).
[43]C. Thomsen, J. Strait, Z. Vardeny, H. J. Maris, J. Tauc, and J. J. Hauser, Phys. Rev. Lett. **53**, 989 (1984).
[44]R. J. Stoner and H. J. Maris, Phys. Rev. B **48**, 16373 (1993).
[45]E. T. Swartz and R. O. Pohl, Rev. Mod. Phys. **61**, 605 (1989).
[46]J. C. Duda, T. Beechem, J. L. Smoyer, P. M. Norris, and P. E. Hopkins, J. Appl. Phys. **108**, 073515 (2010).
[47]G. Gilat and R. M. Nicklow, Phys. Rev. **143**, 487 (1966).
[48]W. Weber, Phys. Rev. B **15**, 4789 (1977).
[49]E. S. Landry and A. J. H. McGaughey, Phys. Rev. B **80**, 165304 (2009).
[50]J. C. Duda, P. E. Hopkins, J. L. Smoyer, M. L. Bauer, T. S. English, C. B. Saltonstall, and P. M. Norris, Nanoscale Microscale Thermophys. Eng. **14**, 21 (2010).
[51]P. E. Hopkins, L. M. Phinney, J. R. Serrano, and T. E. Beechem, Phys. Rev. B **82**, 085307 (2010).
[52]D. G. Cahill and R. O. Pohl, Phys. Rev. B **35**, 4067 (1987).
[53]R. C. Zeller and R. O. Pohl, Phys. Rev. B **4**, 2029 (1971).
[54]T. E. Beechem, S. Graham, P. E. Hopkins, and P. M. Norris, Appl. Phys. Lett. **90**, 054104 (2007).
[55]P. E. Hopkins, P. M. Norris, R. J. Stevens, T. Beechem, and S. Graham, J. Heat Transfer **130**, 062402 (2008).
[56]S. P. Hepplestone and G. P. Srivastava, Phys. Rev. B **82**, 144303 (2010).
[57]P. E. Hopkins, J. C. Duda, S. P. Clark, C. P. Hains, T. J. Rotter, L. M. Phinney, and G. Balakrishnan, Appl. Phys. Lett. **98**, 161913 (2011).
[58]R. N. Salaway, P. E. Hopkins, P. M. Norris, and R. J. Stevens, Int. J. Thermophys. **29**, 1987 (2008).
[59]T. Beechem and P. E. Hopkins, J. Appl. Phys. **106**, 124301 (2009).
[60]S. Shin, M. Kaviany, T. Desai, and R. Bonner, Phys. Rev. B **82**, 081302 (2010).
[61]P. K. Schelling, S. R. Phillpot, and P. Keblinski, J. Appl. Phys. **95**, 6082 (2004).